

# The Shape Optimization of the Pneumatic Valve Diaphragms

Jakub Javorik, Michal Stanek

**Abstract**—Our goal was to analyze mechanical behavior of a rubber diaphragm inside a pneumatic valve and the FEM analysis appears as a very appropriate tool for this work. The hyperelastic parameters of the elastomer material of valve diaphragms were measured. Analyses of the diaphragms in working conditions were carried out. Considering the results of these analyses the new shapes of the diaphragms were designed and were verified again by the numerical analyses.

**Keywords**—diaphragm, elastomer, hyperelasticity, optimization, rubber.

## I. INTRODUCTION

WE need to know how the rubber diaphragm will behave in real conditions in a valve. If we would made and test a number of prototypes during design procedure it would be very time and money consuming. The monitoring of the diaphragm behavior in real valve would be next problem and in a many industrial applications it is absolutely impossible to study behavior of the material in real situations [1]-[10].

The diaphragm is made from silicone rubber. The large elastic strain is characteristic for behavior of rubber. The stress-strain relation of elastomers is strongly nonlinear. Such materials are called hyperelastic and we can use a number of hyperelastic material models to simulate this nonlinear behavior today [11].

A big progress in application of the Finite element method for simulation of physical problems was made in last years [12]. All common hyperelastic models are incorporated in FEM systems today and the full application of nonlinear models of elastomers is allowed thanks development of the FEM systems.

We have to measure properties of every particular material for FEM analysis in laboratory tests. The elastomer for diaphragms was tested in two modes - uniaxial and equibiaxial tension [13]-[15] (Fig. 1).

Manuscript received June 23, 2011; Revised version received June 24, 2011. This work is financially supported by the Ministry of Education, Youth and Sports of the Czech Republic under the Research Plan No. MSM 7088352102 and by the European Regional Development Fund under the project CEBIA-Tech No. CZ.1.05/2.1.00/03.0089.

Jakub Javorik is with the Tomas Bata University in Zlin, Nad stranemi 4511, 760 05 Zlin, Czech Republic (phone: +420 576 035 151; fax: +420 576 035 176; e-mail: javorik@ft.utb.cz).

Michal Stanek is with the Tomas Bata University in Zlin, Nad stranemi 4511, 760 05 Zlin, Czech Republic (e-mail: stanek@ft.utb.cz).

The diaphragms are used as components of pneumatic regulatory valves and they will be loaded by compressed air. The movable rod is fixed in the center of each diaphragm. Different pressure on inner and outer side of the diaphragm moves the rod to its upper or lower position and thus some parameters can be regulated by the rod position.

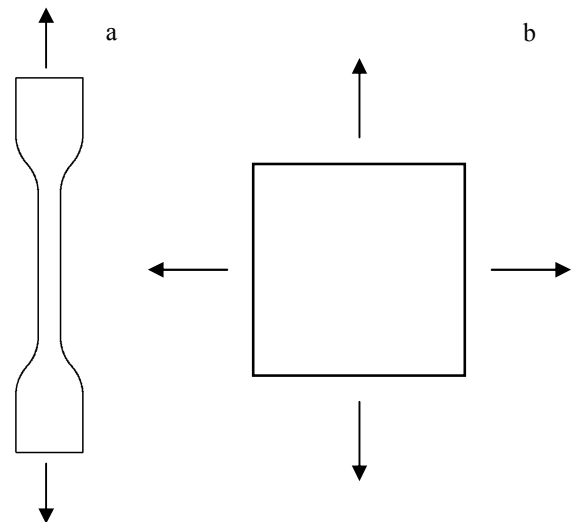


Fig. 1a) uniaxial tension test, b) equibiaxial tension test

## II. MATERIAL AND METHODS

### A. Testing of the Diaphragm Material

For the exact evaluation of hyperelastic material constants, the test data obtained from the uniaxial and equibiaxial tension tests are suitable. The uniaxial tension test was performed on standard testing machine in accordance with ISO 37 standard.

Currently there are not any ISO standard methods for equibiaxial tension test and such tests are rarely performed in industrial laboratories. Thus the bubble inflation technique was used for equibiaxial characterization of diaphragm [14], [15]. In this method a uniform circular specimen of elastomer is clamped at the rim and inflated using compressed air to one side (Fig. 2 and 3). The specimen is deformed to the shape of bubble. The inflation of the specimen results in an equibiaxial stretching near the pole of the bubble and in the planar tension near the rim. The inflation of the specimen and current value of pressure is recorded in short time intervals using a high resolution digital camera.

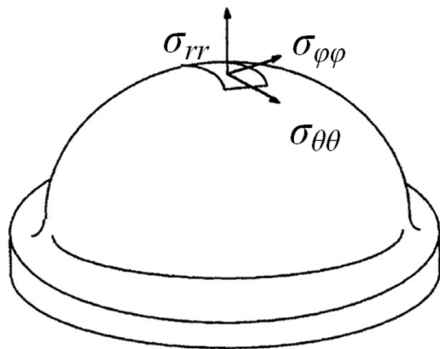


Fig. 2 bubble inflation technique

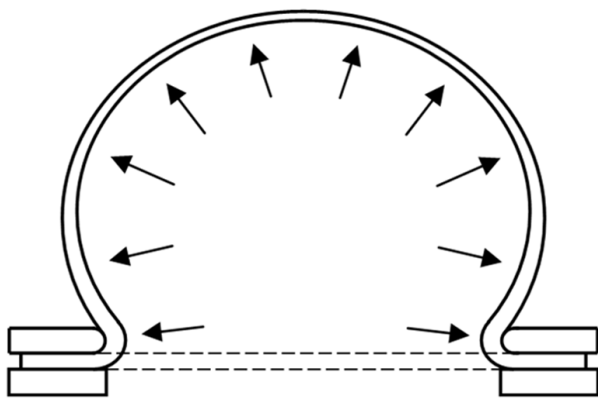


Fig. 3 the specimen inflation

Obtained stress-strain relations for uniaxial and equibiaxial tension of diaphragm material are shown in Fig. 4.

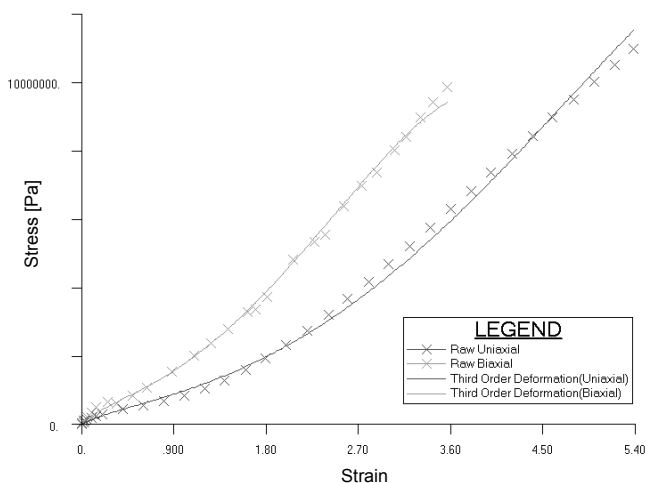


Fig. 4 stress-strain diagram of experimental data and hyperelastic material model

Thanks to the spherical symmetry we can consider  $\sigma_{\theta\theta} = \sigma_{\phi\phi}$  at the pole of the bubble. Then we can write the Cauchy stress tensor in spherical coordinates as:

$$\sigma = \begin{bmatrix} \sigma_{rr} & 0 & 0 \\ 0 & \sigma_{\theta\theta} & 0 \\ 0 & 0 & \sigma_{\theta\theta} \end{bmatrix}_{(r,\theta,z)} \tag{1}$$

The thickness of specimen is small and the ratio between the thickness of the inflated membrane  $t$  and the curvature radius  $r$  is small enough, then the thin shell assumption allow us to neglect the radial stress  $\sigma_{rr}$  in front of the stress  $\sigma_{\theta\theta}$ . In addition we equate  $\sigma_{\theta\theta}$  to the thickness-average hoop stress, which leads to:

$$\sigma_{\theta\theta} = \frac{pr}{2t} \tag{2}$$

where  $p$  is the differential inflation pressure,  $r$  is curvature radius of specimen and  $t$  is the specimen thickness.

With consideration of material incompressibility we can express the thickness of inflated specimen as:

$$t = \frac{t_0}{\lambda_{\theta\theta}^2} \tag{3}$$

where  $t_0$  is the initial thickness of specimen (unloaded state). Further we have to measure the stretch  $\lambda_{\theta\theta}$  at the pole of inflated material. Generally stretch  $\lambda$  is the ratio between the current length  $l$  and the initial length  $l_0$ :

$$\lambda = \frac{l}{l_0} \tag{4}$$

We can use some of optical method for measurement of stretch  $\lambda_{\theta\theta}$  and curvature radius  $r$  (camera, video camera, laser etc.).

Substituting (3) into (2) we can compute the hoop stress  $\sigma_{\theta\theta}$  as:

$$\sigma_{\theta\theta} = \frac{pr\lambda_{\theta\theta}^2}{2t_0} \tag{5}$$

**B. Material Model**

The James-Green-Simpson (by another name 3<sup>rd</sup> order deformation) hyperelastic model was able to fit experimental data of used silicone rubber most closely and was chosen for analysis (Fig. 4). The strain energy density function  $W$  for this model is in the following form:

$$W = c_{10}(J_1 - 3) + c_{01}(J_2 - 3) + c_{11}(J_1 - 3)(J_2 - 3) + c_{20}(J_1 - 3)^2 + c_{30}(J_1 - 3)^3 \tag{6}$$

Measured coefficients (in Pa) for this model are:  $c_{10} = 510140$ ;  $c_{01} = 70468.1$ ;  $c_{11} = -946.852$ ;  $c_{20} = 36418.3$ ;  $c_{30} = -234.302$ , error of model is 1.822.

$J_1$  and  $J_2$  are the first and second deformation invariants

$$J_1 = \lambda_1^2 + \lambda_2^2 + \lambda_3^2 \tag{7}$$

$$J_2 = \lambda_1^2 \lambda_2^2 + \lambda_2^2 \lambda_3^2 + \lambda_3^2 \lambda_1^2 \tag{8}$$

We can derive the stress from the strain energy function as

$$S_{ij} = 2 \frac{\partial W}{\partial C_{ij}} \tag{9}$$

where  $S_{ij}$  is tensor of 2<sup>nd</sup> Piola Kirchhoff stress and  $C_{ij}$  is right Cauchy-Green deformation tensor.

### III. ANALYSIS OF DIAPHRAGMS

Three different diaphragms were analyzed. They are used in regulating pneumatic valves and all have axisymmetric circular shape. They all are made from the same material characterized in the previous chapter. Diaphragms are marked as I, II and III in the following text.

#### A. Analysis of the Diaphragm - I

Initial shape of the first diaphragm is shown in Fig. 5 and 6. Diameter of the diaphragm is 70 mm, height is 12 mm and diaphragm thickness is 0.3 mm. Maximum stress value in the diaphragm must not exceed 2.5 MPa.

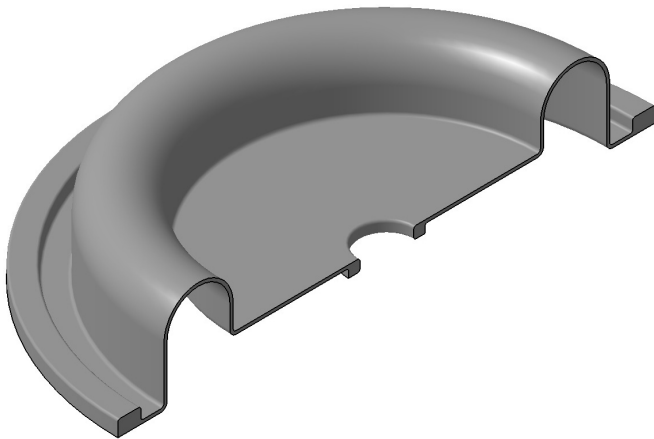


Fig. 5 half-model of the initial design of diaphragm – I

Due to the fact that the diaphragm has axisymmetric shape it is very useful to create 2D axisymmetric FEM model. The diaphragm is mounted on the rod in center of valve and the outer rim of the diaphragm is clamped between two parts of valve body (Fig. 6).

Both parts of the valve body and the rod are modeled as absolutely rigid. The diaphragm is modeled as hyperelastic using material model (1) described above. Analysis consists of four steps (Fig. 6). The rod moves right in first step. In other words the diaphragm is mounted on the rod. Part II of valve

body moves down in second step. The diaphragm is fixed in basic position in valve now. The rod is moved to its upper position in third step and pressure is applied in last step because maximum of pressure can occur only when the rod is up.

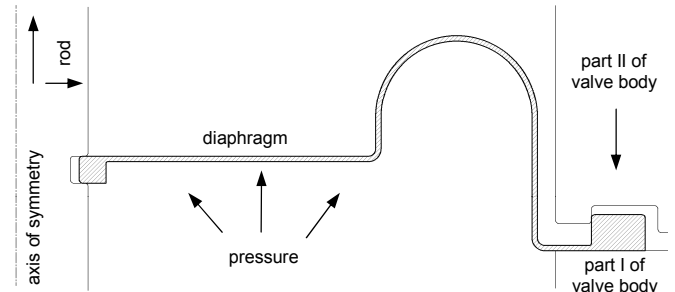


Fig. 6 initial shape of the diaphragm, its boundary conditions and loading

Two criteria were used for results evaluation: maximum stress in the diaphragm (2.5 MPa) and functionality of the diaphragm. It means that the diaphragm must stay fixed in all other parts (the rod and the body of valve) during maximal loading and it must remain hermetic.

First critical point of initial design is located at the rim of diaphragm and it is shown in Fig. 7. This situation occurs at the end of second step. Next two steps were not carried out because very high stress (12 MPa) arose here. It is evident from Fig. 7 that there is not enough space in the groove of valve body for deformation of the diaphragm rim. Thus the enlargement of this groove was the first modification of design.



Fig. 7 results of initial design of diaphragm (after 2<sup>nd</sup> step) – Von Mises stress [Pa]

Results of the second version of design are shown in Fig. 8. Problem at the outer rim was solved and the maximum stress in this area is 1.5 MPa.

The most critical point in the second version is near the central rim of the diaphragm. Its position is pointed as A in Fig. 8 and stress maximum (4.5 MPa) is located here. We can also see that the rim of the diaphragm is almost pulled out from the rod groove. But we can find others points where stress values are locally much higher than stress in their vicinity (points B and C in Fig. 8). Although stress does not exceed 2.5 MPa in these points we can reduce stress values by next modification of shape of the diaphragm. The two corners

of the initial shape are reason of stress concentration in these areas.

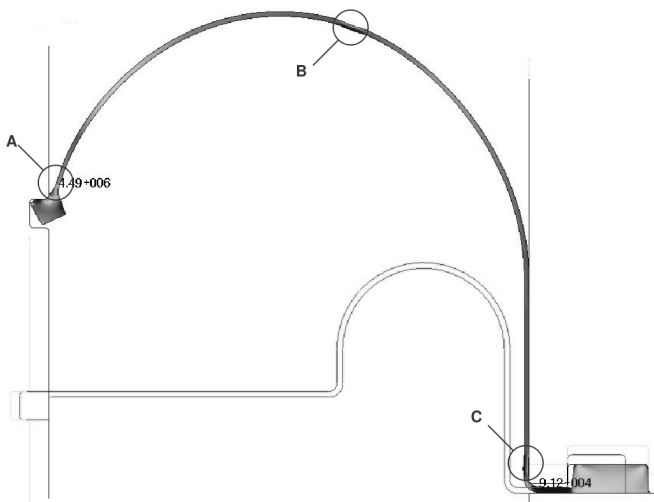


Fig. 8 results of second version of design (after 4<sup>th</sup> step)

With consideration of these results the final shape modifications were done: for point A – widening diaphragm thickness close to central rim and increasing the depth of rod groove; for point B – elimination of corner; and for point C – increasing corner radius (Fig. 9).

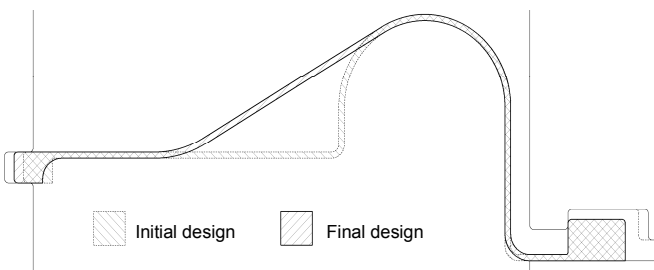


Fig. 9 Final shape of the diaphragm

The shape shown in Fig. 9 was taken as the final design because its analysis did not reveal any critical points. The stress maximum of this shape is located in the same point as in previous version, but its value was significantly reduced to 2.3 MPa (Fig 10 and 11). Also the central rim is much steadier in the rod groove.

Reduction of stress in points B (Fig. 12 and 13) and C (Fig. 14 and 15) was reached too. Nevertheless it is not as significant as in case of the central rim (point A).

The final optimized shape of the diaphragm I is shown in the Fig. 16.

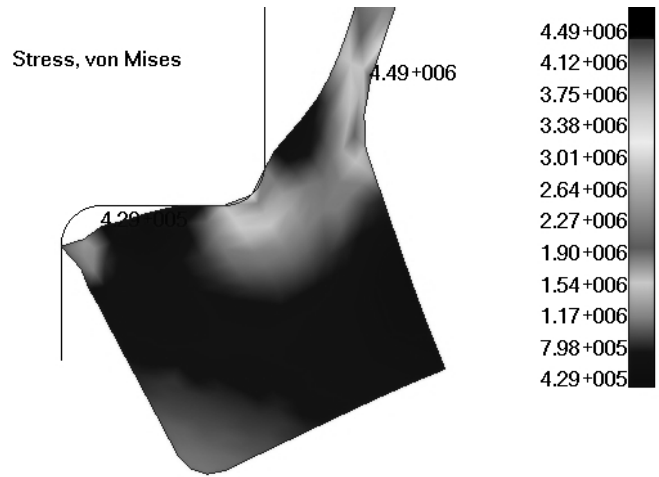


Fig. 10 critical point A in the initial design of diaphragm I – Von Mises stress [Pa]

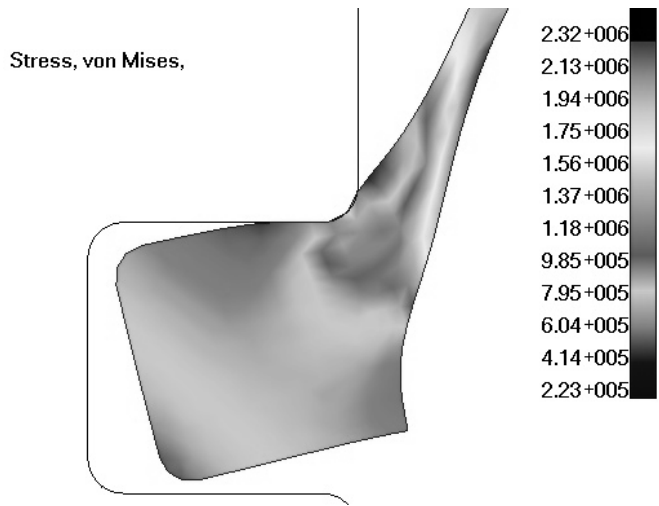


Fig. 11 critical point A in the final design of diaphragm I – Von Mises stress [Pa]

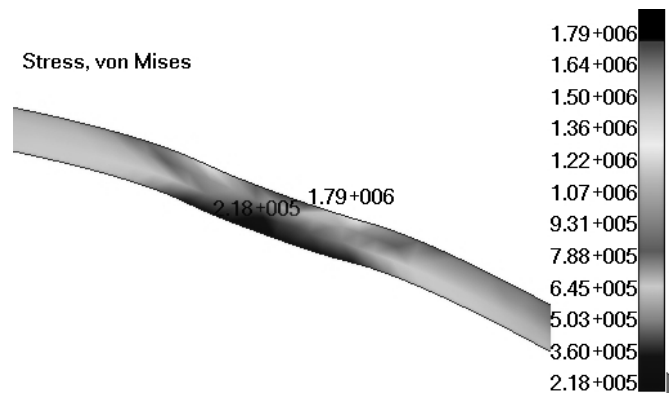


Fig. 12 critical point B in the initial design of diaphragm I – Von Mises stress [Pa]

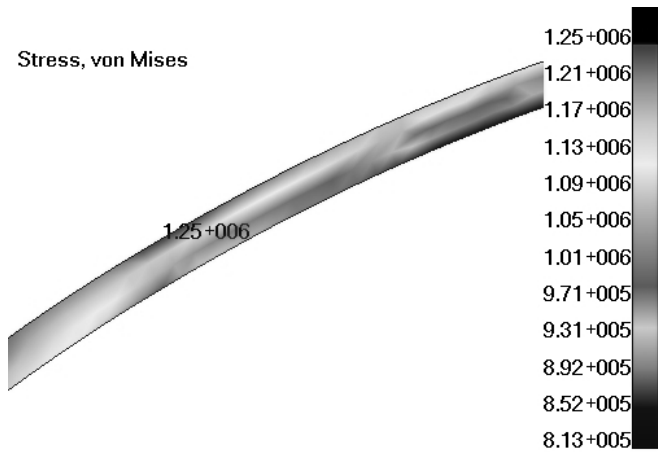


Fig. 13 critical point B in the final design of diaphragm I – Von Mises stress [Pa]

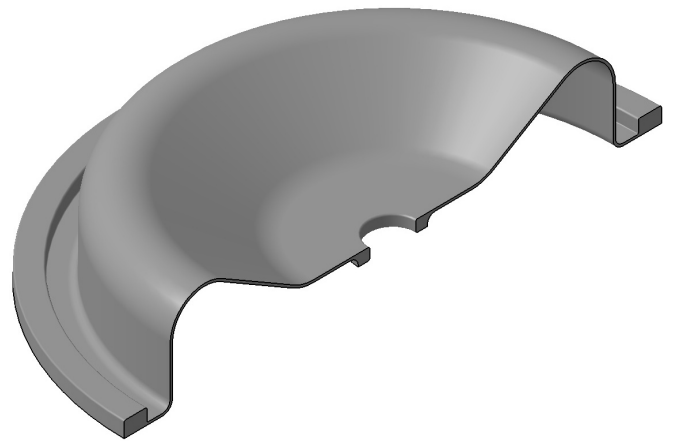


Fig. 16 half-model of the final design of diaphragm – I

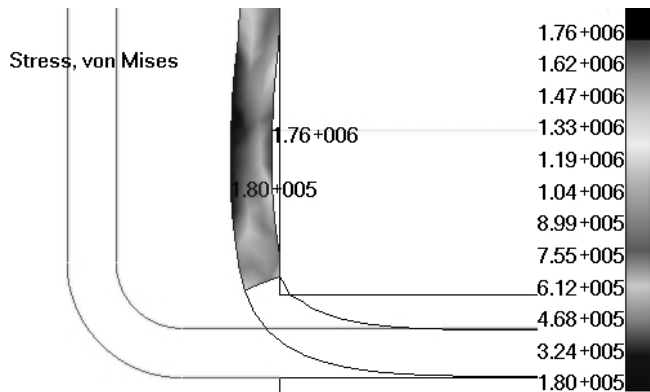


Fig. 14 critical point C in the initial design of diaphragm I – Von Mises stress [Pa]

*B. Analysis of the Diaphragm - II*

Initial shape of the first diaphragm is shown in Fig. 17. Diameter of the diaphragm is 38 mm, height is 18 mm and diaphragm thickness is 0.25 mm. Maximum stress value in the diaphragm must not exceed 2.5 MPa as in the previous case.

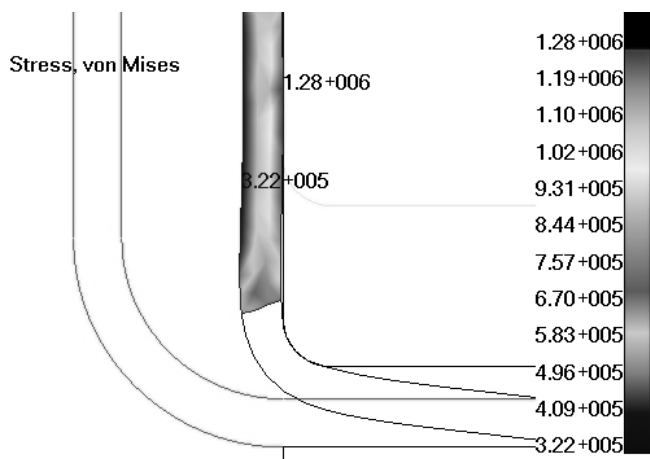


Fig. 15 critical point C in the final design of diaphragm I – Von Mises stress [Pa]

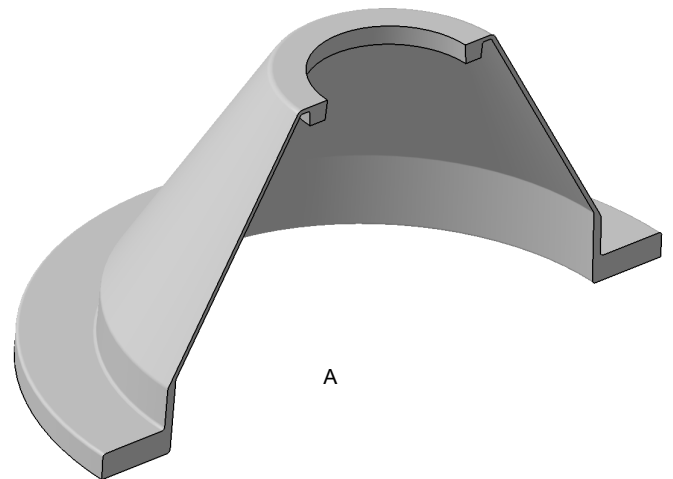


Fig. 17 half-model of the initial design of diaphragm – II

First steps in analysis process are the same as with the diaphragm I. Outer rim of the Diaphragm is clamped between two rigid parts of the valve body and the central rim is mounted in the groove of the movable central rod (Fig. 18). Difference from the diaphragm I is in the loading. Diaphragm II is not loaded by the pressure but only by the moving of the central rod to the utmost position (Fig. 20). The values of the pressure are negligible in this case.

Global maximum of Von Mises stress is on the outer rim of the diaphragm (point A in the Fig. 18) and the reason of this is inappropriate geometry of grooves in which the rim is clamped. The value of Von Mises in this point is 3.3 and exceeds criterion: 2,5 MPa. Solution of this was modification of the valve body design and because the profile of the diaphragm was not changed this is not further discussed.

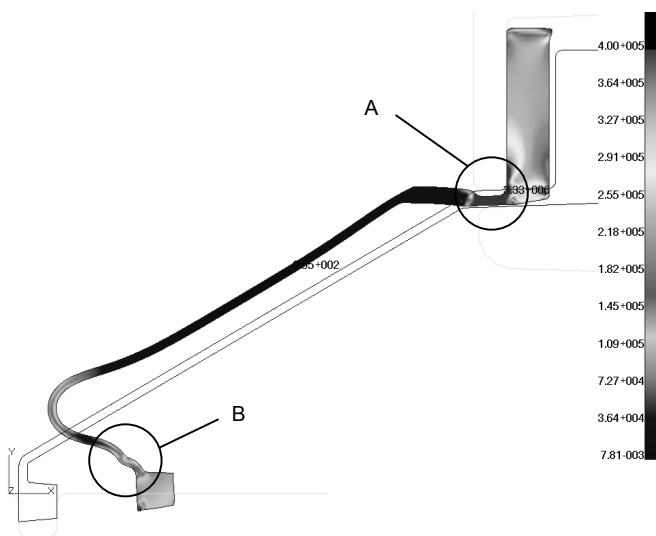


Fig. 18 initial profile of the diaphragm II and its mounting to the basic position in valve – Von Mises stress [Pa]

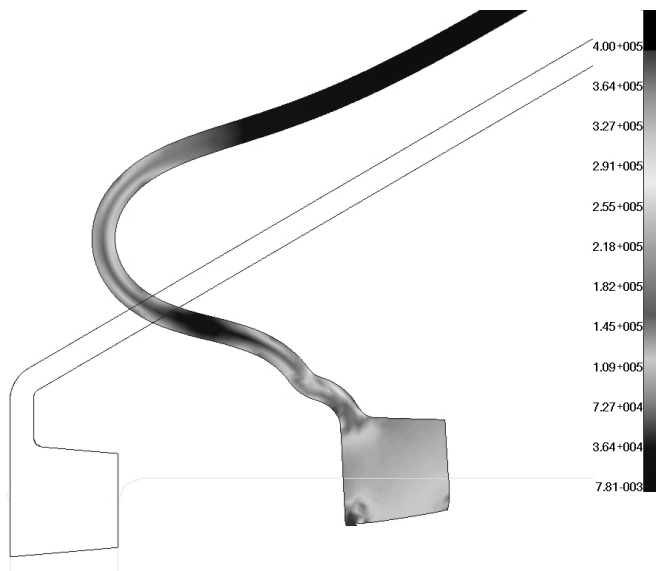


Fig. 19 detail of the mounted central rim of the diaphragm II – Von Mises stress [Pa]

We focused on the next critical point in the diaphragm profile that is signed as B in the Fig. 18. Detail of this part of the diaphragm is shown in the Fig. 19. Values of Von Mises stress there are slightly lower than global maximum in point A but still they are above the criterion of 2.5 MPa.

In Fig. 20 we can see the deformation of the diaphragm after moving the central rod to the uttermost position. The interesting fact is that the stress in the point B (near the central rim) in this case is lower than in the basic position of the diaphragm (Fig. 18). It means that the most critical state is in the basic position and the diaphragm should be optimized for this case.

To decrease stress in point B we decided to increase the thickness of the diaphragm near the central rim and to change

the geometry of the sharp corner in the diaphragm profile in this point as can be seen in Fig. 21. These changes lead to the decreasing the stress values under the 2.5 MPa in the area B and to such shape of the diaphragm that allows more easy and fluent deformation during the moving of the central rod of valve.

The detail of the optimized shape of the central area in the basic position is shown in the Fig. 22 and can be compared with the initial design in the Fig. 19. Deformation of the optimized diaphragm in the uttermost position of the rod is shown in the Fig. 23 and the comparison with the initial situation in the Fig. 18 is again possible.

The final optimized shape of the diaphragm II is shown in the Fig. 24.

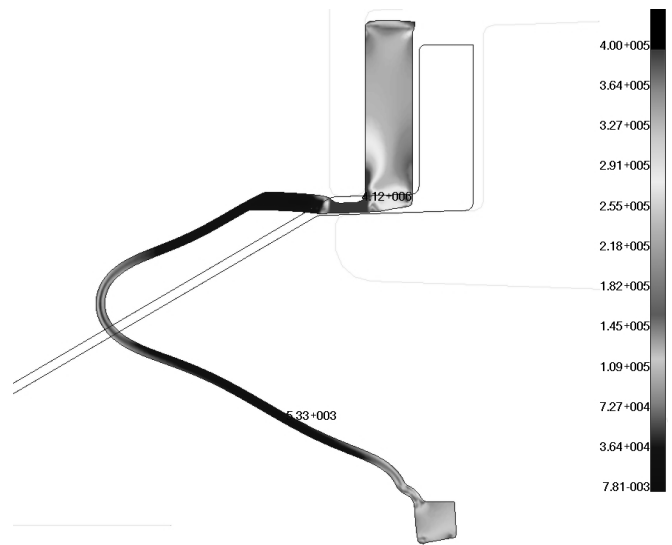


Fig. 20 initial profile of the diaphragm II moved to the uttermost position – Von Mises stress [Pa]



Fig. 21 final profile of the diaphragm II and its mounting to the basic position in valve – Von Mises stress [Pa]

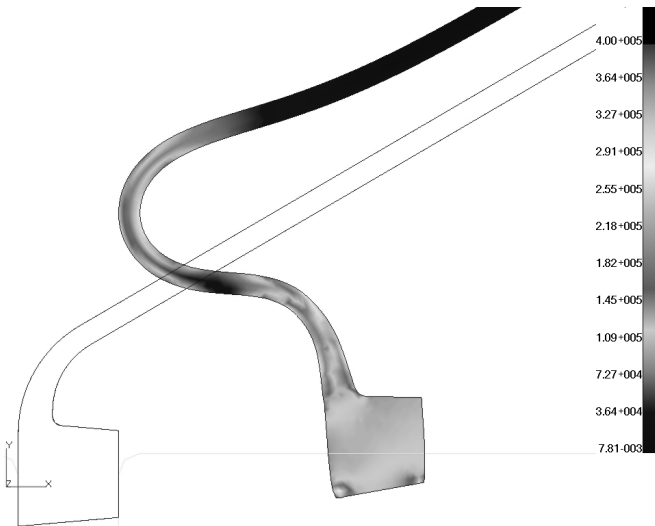


Fig. 22 detail of the mounted central rim of the optimized diaphragm II – Von Mises stress [Pa]

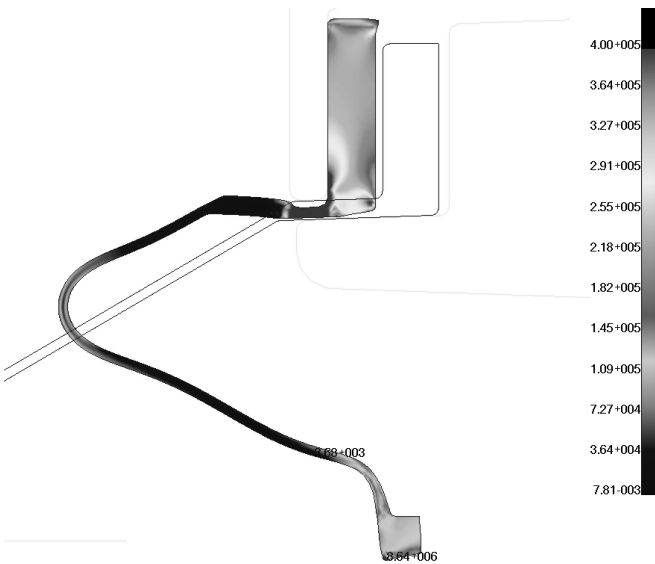


Fig. 23 final profile of the diaphragm II moved to the uttermost position – Von Mises stress [Pa]

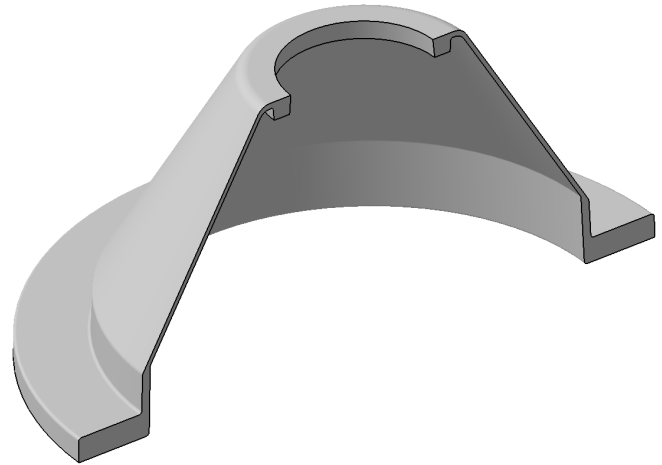


Fig. 24 half-model of the final design of diaphragm – II

### C. Analysis of the Diaphragm - III

Initial shape of the first diaphragm is shown in Fig. 25. Diameter of the diaphragm is 98.5 mm, height is 21.3 mm and diaphragm thickness is 0.3 mm. Maximum stress value in the diaphragm must not exceed 2.5 MPa as in the previous cases.

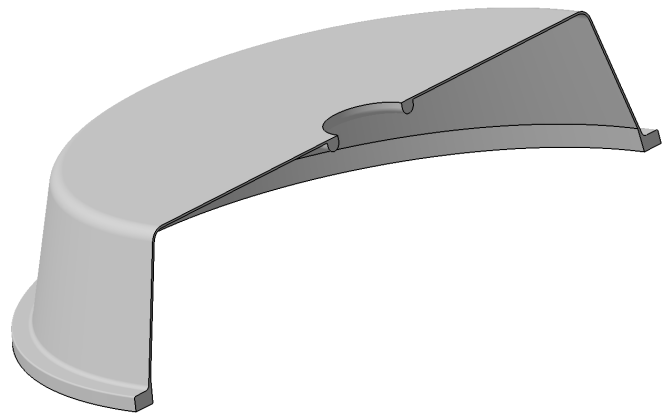


Fig. 25 half-model of the initial design of diaphragm – III

The outer rim of the diaphragm is clamped in the valve body by the same way as in both previous cases. But for the mounting of the central rim on the rod, two flat disks are used. They can be partially seen in the Fig. 26. The whole flat central part of the diaphragm is clamped between these two disks and they are together with the diaphragm mounted on the central rim. It means that opposite to the previous cases the central rim of the diaphragm is not in the groove but it is only pushed to the rod surface.

After the application of the pressure on the lower side of the diaphragm too large deformation of the diaphragm was observed (Fig. 27). Next problem occurs in the center of the diaphragm where the gap between the diaphragm rim and the rod arise (Fig. 28). Thus the new shape of the lower clamping disk was designed and the thickness of the diaphragm was increased from 0.3 mm to 0.4 mm. The results of the analysis of the final shape of diaphragm can be seen in the Fig. 30.

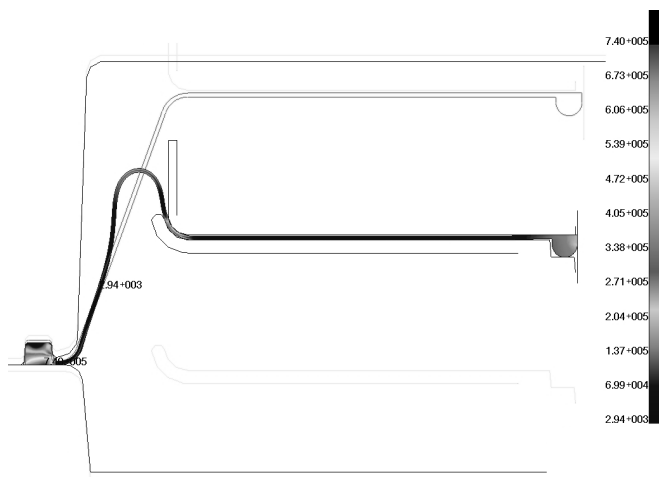


Fig. 26 initial profile of the diaphragm III clamped between disks – pressure is not applied – Von Mises stress [Pa]

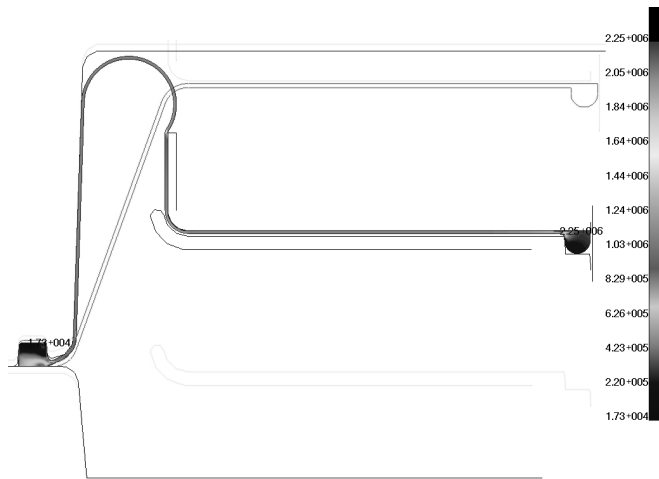


Fig. 27 initial profile of the diaphragm III clamped between disks with the pressure applied – Von Mises stress [Pa]

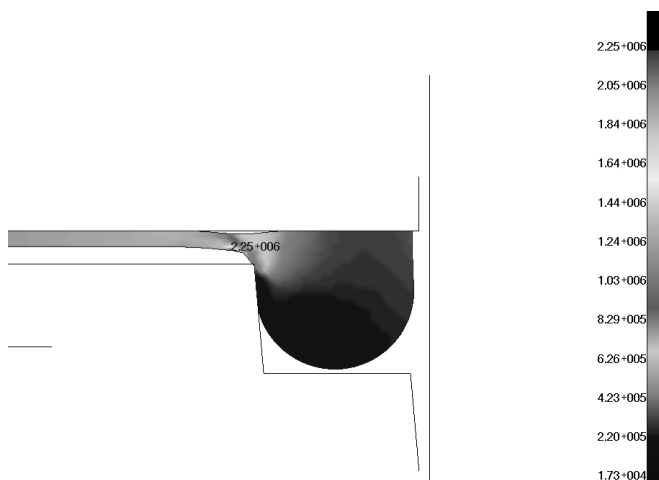


Fig. 28 central part of the initial design of the diaphragm III –

Von Mises stress [Pa]

After the analysis of the final profile of the diaphragm III the stress values did not exceed 0.9 Mpa. This value is very small in comparison with the strength of the material (2.5 Mpa) and thus there was not need to change the shape due to the stress.

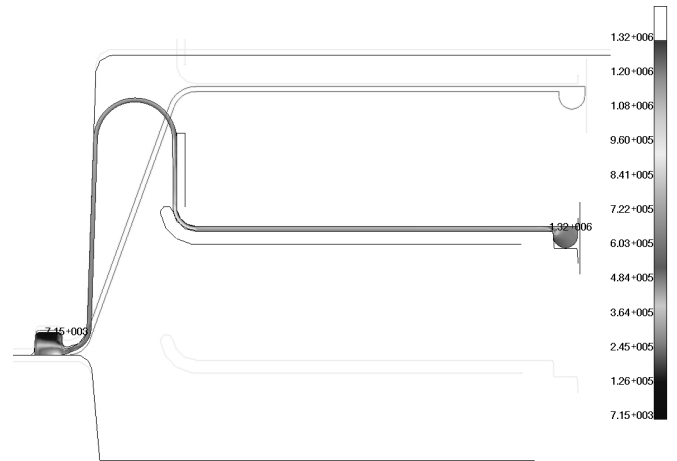


Fig. 29 deformation of the final profile of the diaphragm III clamped between original disks with the pressure applied – Von Mises stress [Pa]

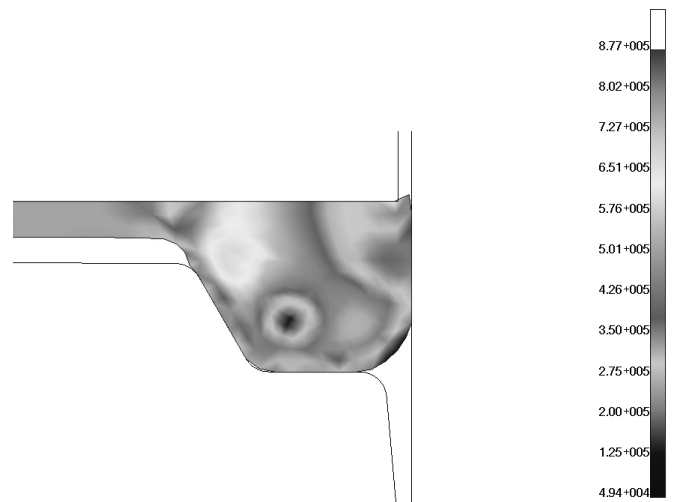


Fig. 30 central part of the final design of the diaphragm III – Von Mises stress [Pa]

IV. CONCLUSION

All criteria for the diaphragm I were fulfilled and the final design of the diaphragm was created. Three versions of the diaphragm I were analyzed – initial, second and final version. The enlargement of groove in valve body was necessary after analysis of the initial version. The next model (second version) with this modification was created and analyzed. With consideration of results of second version the rod groove was deepened and the shape of diaphragm I was changed (final version – Fig. 9). The analysis of this modified shape proved

that there are not exceeded stress/strain limits in the final version of diaphragm. Deformation does not exceed limit even in the initial model. But high stress was the reason of shape modification for the final version. The point, where stress maximum is reached in diaphragm I, is near to the central rim (Fig. 8A).

At first the geometry of the groove for the outer rim of the diaphragm II in the valve body was changed. And finally the thickness of the diagram II near the central rim was increased and the geometry of the diagram profile in this point was changed.

The thickness and the shape of the lower clamping disk for the diaphragm III were modified. The inappropriate deformation of the diaphragm was the reason of these modifications. The stress value was under the limit and there was not need to other changes in the diaphragm.

- I: Experimental Investigations," *Polymer Engineering and Science*, issue 3, vol. 41, 2001, pp. 522-531.  
 [15] J. Javorik, Z. Dvorak, "Equibiaxial test of elastomers," *KGK – Kautschuk Gummi Kunststoffe*, issue 11, vol. 60, 2007, pp. 608-610.

#### REFERENCES

- [1] A. Arghiropol, C. Rotaru, "Overview of the 2D and 3D Finite Element Studies versus Experimental Results of a Solid Propellant Engine Performances under Cycling Loading Effect," *International Journal of Mathematics and Computers in Simulation*, issue 2, vol. 4, 2010, pp. 42-49.
- [2] S. Amornsamankul, K. Kaorapapong, B. Wiwatanapataphee, "Three-Dimensional Simulation of Femur Bone and Implant in Femoral Canal using Finite Element Method," *International Journal of Mathematics and Computers in Simulation*, issue 4, vol. 4, 2010, pp. 171-178.
- [3] M. C. Popescu, M. E. Mastorakis, "Optimal Flow Control of a Three Tank System," *International Journal of Mathematics and Computers in Simulation*, issue 4, vol. 3, 2009, pp. 179-186.
- [4] J. Javorik, M. Stanek, "The Numerical Simulation of the Rubber Diaphragm Behavior," in *Proc. 13<sup>th</sup> WSEAS International Conference on Automatic Control, Modelling & Simulation*, Lanzarote, Spain, 2011, pp. 117-120.
- [5] J. Javorik, D. Manas, "The Specimen Optimization for the Equibiaxial Test of Elastomers," in *Proc. 13<sup>th</sup> WSEAS International Conference on Automatic Control, Modelling & Simulation*, Lanzarote, Spain, 2011, pp. 121-124.
- [6] O. Suba, L. Sykorova, S. Sanda, M. Stanek, "Modeling of Thermal Stress in Printed Circuit Boards," in *Proc. 13<sup>th</sup> WSEAS International Conference on Automatic Control, Modelling & Simulation*, Lanzarote, Spain, 2011, pp. 173-176.
- [7] O. Suba, L. Sykorova, S. Sanda, M. Stanek, "Stress-State Modelling of Injection-molded Cylindrical Bosses Reinforced with Short Fibres," in *Proc. 13<sup>th</sup> WSEAS International Conference on Automatic Control, Modelling & Simulation*, Lanzarote, Spain, 2011, pp. 177-179.
- [8] L. Sykorova, O. Suba, M. Malachova, J. Cerny "Temperature Field Simulation of Polymeric Materials During Laser Machining Using CASMOS/M Software," in *Proc. 13<sup>th</sup> WSEAS International Conference on Automatic Control, Modelling & Simulation*, Lanzarote, Spain, 2011, pp. 180-184.
- [9] D. Manas, M. Manas, M. Stanek, M. Zaludek, S. Sanda, J. Javorik, V. Pata, "Wear of Multipurpose Tire Treads," *Chemicke listy*, issue 13, vol. 103, 2009, pp. 72-76.
- [10] D. Manas, M. Stanek, M. Manas, V. Pata, J. Javorik, "Influence of Mechanical Properties on Wear of Heavily Stressed Rubber Parts," *KGK – Kautschuk Gummi Kunststoffe*, issue 5, vol. 62, 2009, pp. 240-245.
- [11] R. W. Ogden, *Non-linear Elastic Deformations*, New York, Dover Publications, 1997.
- [12] A. F. Bower, *Applied Mechanics of Solids*, New York, CRC Press, 2009.
- [13] L. P. Smith, *The language of Rubber*, Oxford, Butterworth-Heinemann, 1993.
- [14] N. Reuge, F. M. Schmidt, Y. Le Maout, M. Rachik, F. Abbe, "Elastomer Biaxial Characterization Using Bubble Inflation technique.